Towards Femtojoule Nanoparticle Phase-Change Memory

Andrey I. Denisyuk, Kevin F. MacDonald, F. Javier García de Abajo[1], and Nikolay I. Zheludev*

Optoelectronics Research Centre, University of Southampton, SO17 1BJ, United Kingdom
[1]*Instituto de Óptica—CSIC, Serrano 121, 28006 Madrid, Spain*

Received September 16, 2008; accepted December 23, 2008; published online March 23, 2009

In this article we review the concept of electron-beam-addressed high density phase-change nanoparticle memory, where information is written in the phase state of gallium nanoparticles by electron beam excitation, and read-out via measurements of cathodoluminescent emission. The high spatial resolution provided by a focused electron beam, far below the optical diffraction limit, offers the possibility of addressing individual nanoparticles within a close-packed array, thereby enabling a new conceptual basis for high density phase-change memory.

DOI: 10.1143/JJAP.48.03A065

1. Introduction

The ultimate goal of nanophotonics, and its sub-field of plasmonics, is to create devices smaller than or comparable in size to the wavelength of the signals they handle (a relationship of proportions that is easily achieved in microelectronics), in particular for data processing and transport applications.[1–4] Such technologies will obviously require nanoscale components for optical switching and data storage.

Numerous approaches have been considered to realize such functionalities. For switching and signal modulation these range from photoinduced carrier excitation in quantum dots[5] to third order nonlinear switching augmented by plasmonic resonances in metallic nanoparticles,[6] and enhanced photoinduced effects in nanoparticle composite media.[7,8]

The optical data storage industry is currently dominated by chalcogenide phase-change media (which can be switched between optically distinguishable crystalline and amorphous states using laser pulses) in the form of compact (CD), digital-versatile (DVD), and Blu-ray discs. There is now rapidly growing interest in phase change materials for next-generation nanoscale optical and electronic switching and memory applications due to their potential to address growing challenges of size and power consumption, and to enable innovative photonic and plasmonic functionalities.[9–11]

Encoding information in a nanoscale volume of material requires a significant change in the absorption or refraction of that volume in response to external control excitations and such changes can be achieved in certain materials via a phase change. For instance, vanadium dioxide nanoparticles are found to show a photoinduced insulator-to-metal transition within a time scale of about 100 fs.[12] Light induced phase-change switching has also been demonstrated using gallium nanoparticles.[13] Indeed, gallium can exist in several phases with markedly different optical properties ranging from those of the almost semiconductor-like, partially covalent solid α phase to those of the highly metallic liquid.[14,15] The solid α phase is not normally found in nanoparticles,[16] but these exist in a variety of other crystalline phases known as β, δ, ϵ, and γ gallium, which have optical properties between those of the α and liquid phases[17] (see gallium phase diagram in Fig. 1 [after Bosio[18]]).

Phase transitions in nanoparticles are characterized by low energy consumption. For example, to convert a spherical 50 nm diameter gallium particle from the β(solid) to the liquid phase requires less than 20 fJ of energy (based on latent heat values from Defrain[17]). Even less energy is required for solid-to-solid structural transformations in gallium. Indeed, the δ and β crystalline phases are only separated by 3×10^{-4} eV/atom,[17] which suggests the possibility of few- or even single-photon per particle switching.[10]

Of crucial importance to the memory functionality of metallic nanoparticles is the nature of the phase transition process itself. In contrast to bulk materials, phase transitions in nanoparticles are characterized by a wide thermal hysteresis where "reverse" transitions from high- to low-energy phases occur at lower temperatures than the corresponding "forward" transitions, thus creating a region where both phases are stable[19–21] (see Fig. 2). In the case of gallium nanoparticles this region of bistability can be up to 100 K wide, providing a solid base for phase-change memory functionality.[22]

Another important question is that of the minimum particle size for which conventional phase transitions remain (before atomic cluster behaviors take over). The theoretical lower limit for gallium particle diameter is 3–4 nm.[23] At this size, if each particle within a close-packed planar array could be addressed individually as binary memory elements, a storage density approaching 50 Tbit/in.^{2} could be achieved (for comparison, Blu-ray disks offer 0.015 Tbit/in.^{2}).

Binary all-optical memory functionality has recently been demonstrated using a gallium nanoparticle film (with the whole film of some 10000 particles on the end face of a single mode optical fiber core acting as a single memory element),[22] and higher-base logic (quaternary) all-optical memory has been demonstrated for a single 100 nm gallium nanoparticle isolated in a nano-aperture at the tip of a tapered, metal-coated optical fiber.[24] In these schemes, single laser pulses (~1 pJ energy per particle) induce lower- to higher-energy structural transformations in the particles (at a temperature within the hysteresis loop) to "write" information to the memory element, and "readout" is achieved through reflective measurements of the particles' linear or nonlinear optical properties.

An electron beam, which can be focused on the nanoscale (far below the diffraction limit for an optical beam), might be used to address individual particles within a nanoparticle film, providing energy to record data by inducing structural

*E-mail address: niz@orc.soton.ac.uk

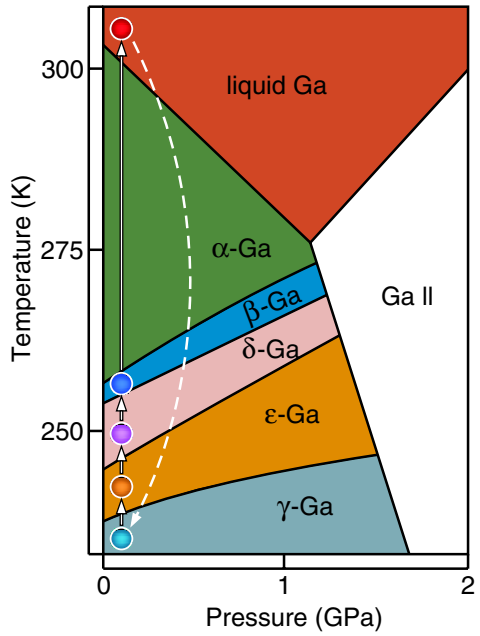

Fig. 1. (Color online) Gallium phase diagram after Bosio[18] with the allowed increasing-energy transition sequence for nanoparticles (γ, ϵ, δ, β, liquid) overlaid. The α phase is not found in nanostructures, so solid–liquid transitions occur between the β form and the melt.

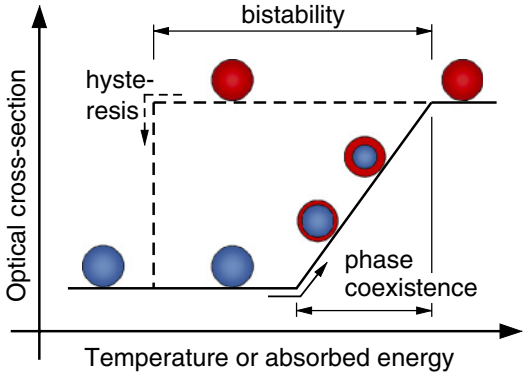

Fig. 2. (Color online) Phase change optical functionality in a nanoparticle: schematic dependence of optical cross-section on absorbed energy for a nanoparticle undergoing a phase transition. The bistability required for memory applications results from a broad thermal hysteresis in the transition.

transitions and enabling readout via measurements of cathodoluminescent (CL) emission (Fig. 3). Indeed, luminescent detection of phase state is used for insulator materials[25] and CL has been used to probe electron-beam induced memory effects in semiconductors.[26,27]

The electron-beam-induced switching of a large planar ensemble of gallium nanoparticles (~10000 particles over an area of 60 μm^2), and associated CL identification of their phase (memory) state has recently been demonstrated.[28] Here we review the entire concept of electron-beam-addressed gallium nanoparticle phase-change memory, from the metal's CL emission characteristics, through size-controlled light-assisted nanoparticle fabrication, to the demonstration of selectively addressed 50-particle memory elements within a nanoparticle film.

2. Experimental Methods

For the purposes of studying phase-change functionality in gallium nanoparticles an integrated experimental setup was developed wherein samples could be prepared under high-vacuum, temperature-controlled conditions, then imaged and probed by both optical and electron beams *in situ*. The system was based on a modified scanning electron microscope (SEM; Fig. 4) equipped with an effusion cell for gallium nanoparticle growth, a liquid-nitrogen-cooled cryostat to control sample temperature in the 90–305 K range and a spectroscopic CL measurement system. The latter comprised a bespoke parabolic mirror positioned directly above the sample (with a hole in for the electron-beam to pass through, collecting emitted light over half of the available hemispherical solid angle), a Horiba Jobin-Yvon CP140 spectrograph and a liquid nitrogen-cooled CCD array for wavelength-sensitive detection in the 400–1000 nm range. A fiber-based optical diagnostic system (described in detail below) entering the SEM chamber via a vacuum feedthrough provided for optical excitation and probing of samples at 1310 and 1550 nm wavelengths.

3. Cathodoluminescence of Bulk Gallium

A preliminary investigation of electron-beam-induced light emission from bulk gallium was performed. This sample was prepared by placing a 1 mm diameter droplet of high-purity (99.9999%) liquid gallium (melting point = 303 K) on the surface of the SEM's cryostatic sample stage [see inset to

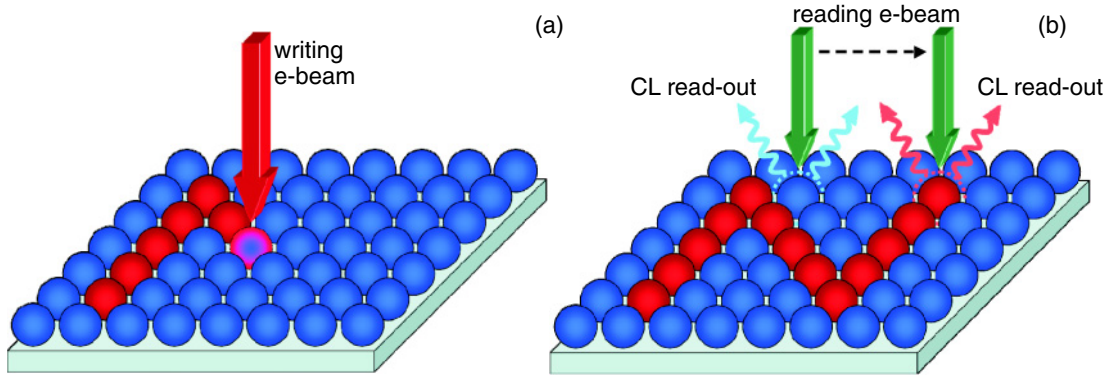

Fig. 3. (Color online) Schematic illustration of (a) writing and (b) CL readout processes in high-density electron-beam-addressed phase-change nanoparticle memory. Phase switching is induced using a higher energy electron beam, CL emission is excited at lower energy.

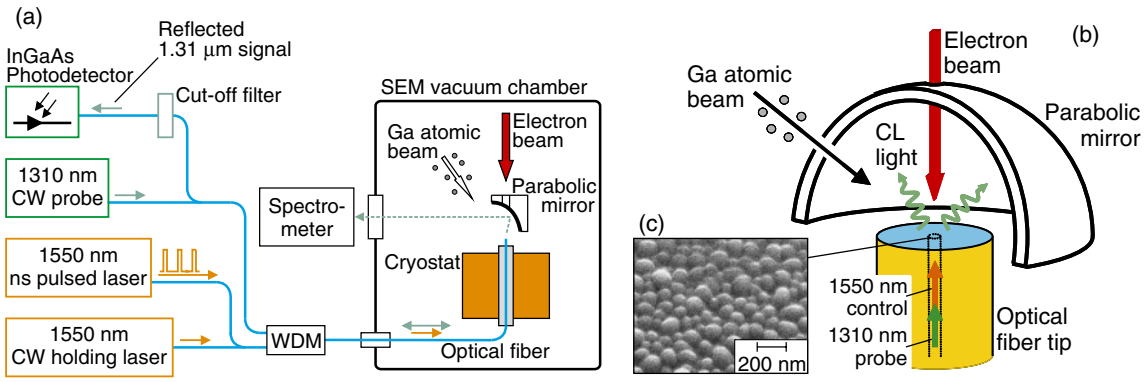

Fig. 4. (Color online) (a) Schematic of the integrated system for growth, imaging, CL study, and optical interrogation of gallium nanoparticle films. (b) Detailed schematic of the arrangement of light-collection mirror and optical fiber substrate. (c) Secondary electron image of a typical gallium nanoparticle film grown in the core area of a cleaved fiber tip.

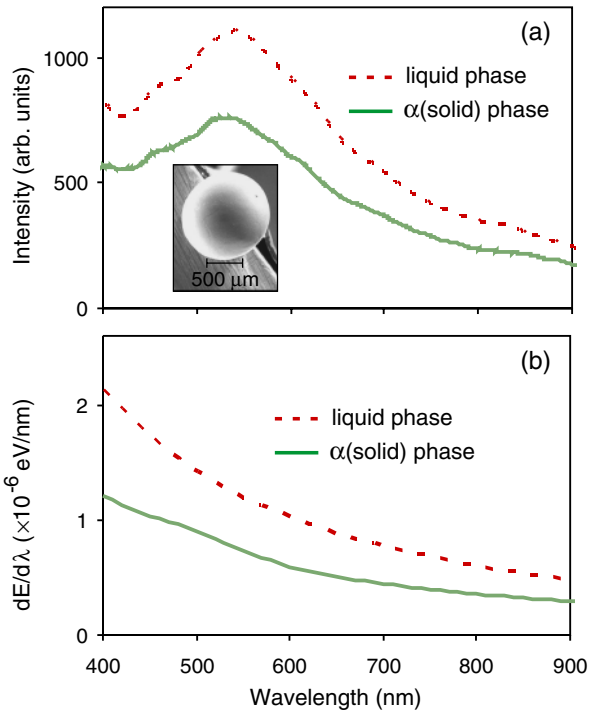

Fig. 5. (Color online) (a) Experimental CL emission spectra (obtained with a 40 keV electron beam) for bulk gallium in the solid α (green line) and liquid (red dashed line) phases. The inset shows a secondary electron image of the gallium droplet. (b) Calculated transition radiation spectra (emitted energy induced by one incident electron) for a 40 keV electron traveling perpendicular to α and liquid gallium/vacuum interfaces.

Fig. 5(a)]. Under vacuum conditions the stage was cooled to 253 K to solidify the droplet, then heated at a rate of 2.5 K/min. Between 283 and 313 K, CL emission spectra were continuously recorded by scanning a $12 \times 9.6\,\mu$m region of the droplet with a 40 keV, 2.9 nA electron beam. At the 303 K melting point of the metal's solid α phase an increase in light emission at all wavelengths (up to 50% in the 550–650 nm range) was observed. Figure 5(a) shows representative CL emission spectra for the solid and liquid phases.

In metals, transition radiation plays the major role in light emission induced by electron bombardment. Plasmon emission decoupled by surface roughness features can also contribute.[29] In the case of gallium there may also be a contribution from recombination emission since the solid α phase shows interband transitions via which light can be emitted between 520 and 1000 nm (2.4–1.25 eV), with a maximum at 540 nm (2.3 eV).[30] Liquid gallium retains some atomic order similar to that of the metastable solid phases[17] and may therefore possess transition bands at similar wavelengths.

Calculations of transition radiation emission, integrated over a hemispherical solid angle of 2π in the backward direction relative to the electron trajectory, were performed using formulae from Ginzburg[31] for 40 keV electrons traveling perpendicular to solid and liquid gallium/vacuum interfaces [Fig. 5(b)]. Dielectric functions used in the calculations were obtained from Kofman *et al.*[32] for α-gallium and from Teshev and Shebzukhov[33] for liquid Ga. In keeping with the experimental results, the calculated emission spectra show markedly higher emission from the liquid phase at all wavelengths and reproduce the increasing strength of emission with decreasing wavelength. The experimentally observed emission peak at 550 nm does not appear and would therefore seem to be associated with recombination emission resulting from interband transitions around this wavelength.

Note that while the maximum penetration depth of 40 keV electrons into gallium is around 7 μm (given by formulae from Kanaya and Okayama[34]), light emission can only come from a surface layer with a thickness limited by the optical skin depth, which is 15 nm for α-gallium and 7 nm for the liquid phase in the 500–550 nm wavelength range. This fact is crucial to the functionality of individual nanoparticles as memory elements.

4. Gallium Nanoparticle Size Control

Aside from the phase-change memory application under discussion here, the preparation of metallic nanoparticles is a technologically important issue for such applications as field-enhanced spectroscopy, catalysis, magnetic nanoparticle memory, and cancer treatment.[35–38] Because the optical, electronic and thermodynamic properties of metallic nanoparticles are strong functions of their size[23,39] it is critical that their production be precisely controlled and highly reproducible. Self-assembly can typically produce particles with a narrow size distribution only up to a mean diameter of

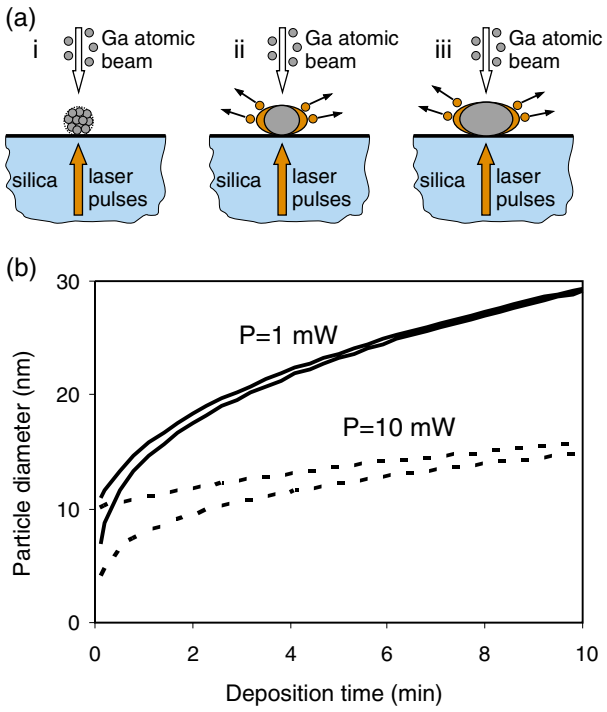

Fig. 6. (Color online) (a) Schematic illustration of the light-assisted self-assembly process for gallium nanoparticles: [i] formation of small clusters, which do not interact with incident IR laser light; [ii] strength of interaction with optical radiation increases with particle aspect ratio, activating selective light-enhanced desorption and light-suppressed adsorption mechanisms; [iii] particle size is controlled by the temperature-, laser power- and atomic beam flux-dependent balance between absorption and desorption. (b) Growth of gallium nanoparticles controlled by light-suppressed adsorption (after Fedotov *et al.*[48]). The dependence of particle diameter on deposition time for 1 and 10 nm seed diameters and laser powers of 1 mW (solid lines) and 10 mW (dashed lines).

around 5 nm, for larger particles the size distributions tend to be bimodal.[40–42] Optical techniques for the post-growth manipulation of nanoparticle shape, size and size distribution (based on evaporation, desorption and fragmentation processes induced by high-power pulsed lasers) have been reported.[43–45] Recently, it has also been shown that low power optical excitation can be used to control nanoparticle growth processes. For example, dual-beam near-UV to visible wavelength illumination can control the growth of colloidal silver nanoprisms,[46] and pulsed infrared excitation has been found to control the growth of substrate-supported gallium nanoparticles from atomic beam.[47]

The light-assisted self-assembly process for gallium particles subject to pulsed infrared laser excitation proceeds as follows:[47,48] Deposition from an atomic beam onto a silica substrate cooled to 100 K results in the growth of solid-phase nanoparticles. Atomic clusters are initially formed [Fig. 6(a-i)] and because gallium wets silica rather well these grow preferentially across the substrate surface, increasing their diameter-to-height aspect ratio. The IR absorption cross-section of the particles depends strongly on their size and aspect ratio so as they grow the strength of their interaction with the incident laser light increases [Fig. 6(a-ii)]. This increasing absorption activates two processes: light-enhanced desorption, whereby IR excitation promotes desorption of atoms from particles' surfaces by breaking bonds within the metal's solid structure, and light-suppressed adsorption, whereby the probability of successful binding for new atoms arriving from the atomic beam is reduced in optically excited particles [Fig. 6(b)]. The dynamic balance between these processes, which depends on substrate temperature, laser power and atomic beam flux, controls the size and narrows the size distribution of particles during growth [Fig. 6(a-iii)].

A systematic study of the light-assisted gallium nanoparticle formation process has been conducted, focusing in particular on the influence of laser power, deposition time and substrate temperature on the particles obtained. Nanoparticles were grown for between 22.5 and 67.5 min with an atomic beam flux of 0.3 nm/min on the end face of a cleaved single-mode optical fiber (SMF-28) at a temperature of 90 or 105 K. During growth the particles were exposed [via the fiber, see Fig. 4(a)] to light from a pulsed 1550 nm erbium-doped fiber laser producing 3 ns pulses at a repetition rate of 20 kHz with an average power of between 0.1 and 0.8 mW. During deposition the reflectivity of the film was monitored using a low power (0.5 mW) continuous beam from a 1310 nm diode laser. After growth the sample stage was brought to room temperature and images of the particle film were acquired (Fig. 7).

A number of depositions were performed for 45 min with a cryostat temperature of 90 K and with average laser powers ranging from 0.1 to 0.8 mW [average intensities of 160 to 1260 W/cm^2 in the fiber core, Figs. 7(a)–7(d)]. It was found that for laser powers up to 0.4 mW (intensity 630 W/cm^2) the mean diameter of the nanoparticles obtained decreased with increasing power (from 68 nm at 0.1 mW to 45 nm at 0.4 mW), in keeping with the theoretical model described above and by Fedotov *et al.*[48] The size distribution histograms also show that the nanoparticle films obtained at 0.2 and 0.4 mW are considerably more monodisperse than that obtained at 0.1 mW, which has a bimodal size distribution.

Further increasing the incident optical power to 0.8 mW (an average intensity of 1260 W/cm^2) produces a disorganized film of partially merged nanoparticles with a median diameter of 57 nm. This is explained by the heating effect of the laser light (not accounted for in the theoretical model): at 0.8 mW it is sufficient to melt the particles during growth, allowing them to coalesce.

At a fixed temperature of 90 K and average laser power of 0.2 mW, further depositions were performed with durations of 22.5 min (0.5 times the 45 min employed above) and 67.5 min (1.5 times 45 min) [Figs. 7(e) and 7(f)]. The mean particle diameter is found to increase with deposition time (from 37 nm at 22.5 min to 53 nm at 45 min and 75 nm at 67.5 min), and at the same time the size distribution narrows (standard deviation as a percentage of mean diameter changes from 33 to 28%). The theoretical model predicts both of these trends.

An additional deposition was performed at an average laser power of 0.2 mW for 45 min but with an increased substrate temperature of 105 K [Fig. 7(g)]. While the theoretical model (which assumes solid phase growth) predicts a decrease in particle size with increasing temper-

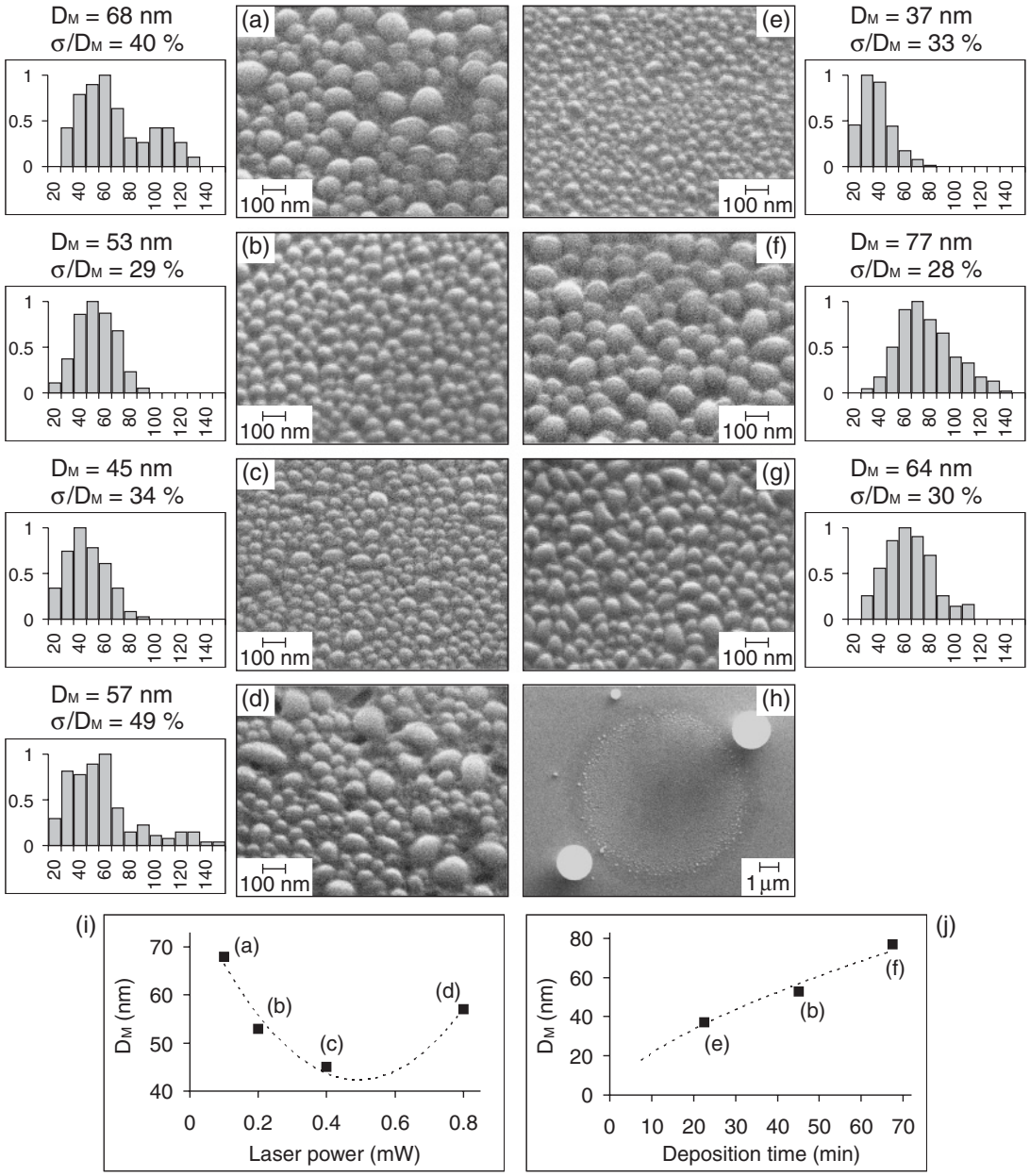

Fig. 7. Secondary electron images of gallium nanoparticle films obtained under varying conditions of average incident laser power, substrate temperature and deposition time: (a) 0.1 mW, 90 K, 45 min; (b) 0.2 mW, 90 K, 45 min; (c) 0.4 mW, 90 K, 45 min; (d) 0.8 mW, 90 K, 45 min; (e) 0.2 mW, 90 K, 22.5 min; (f) 0.2 mW, 90 K, 67.5 min; (g) 0.2 mW, 105 K, 45 min with corresponding histograms of particle size distribution (diameter in nm), mean diameters (D_M), and standard deviations (σ) as a percentage of mean diameter. (h) lower magnification image showing the core area of a fiber tip, where uniformly sized nanoparticles are formed under the influence of laser radiation, and the surrounding area where large and disorganized structures are deposited. (i) Dependence of nanoparticle mean diameter on laser power. (j) Dependence of nanoparticle mean diameter on deposition time.

ature, in the present case it is found that the mean diameter increases from 53 nm at 90 K to 64 nm at 105 K. It is noticeable that the 105 K film contains numerous non-spheroidal particles suggesting that at this temperature they grew in the liquid phase and were able to begin coalescing (as above for the 90 K deposition with 0.8 mW laser excitation).

Outside the core area of the fiber, where deposited material is not exposed to laser radiation, the growth process is uncontrolled. Figure 7(h) shows the core and surrounding area of a typical fiber end face after gallium deposition — in this case a number of large, micrometer size particles are formed outside the core.

5. Nanoparticle Phase-Change Memory Functionality

For a proof-of-principle demonstration of phase-change nanoparticle memory a sample of the type shown in Fig. 7(b) (relatively monodisperse with a mean diameter of 53 nm) was selected. Data was encoded in the structural phase of the particles: solid phase = logic state "0", liquid phase = logic state "1". We report here on a volatile mode of operation, with the holding power required to retain written data provided by a 3 mW continuous-wave (cw) 1550 nm diode laser. Writing (from state "0" to "1") was achieved using single-pulse 20 keV electron beam

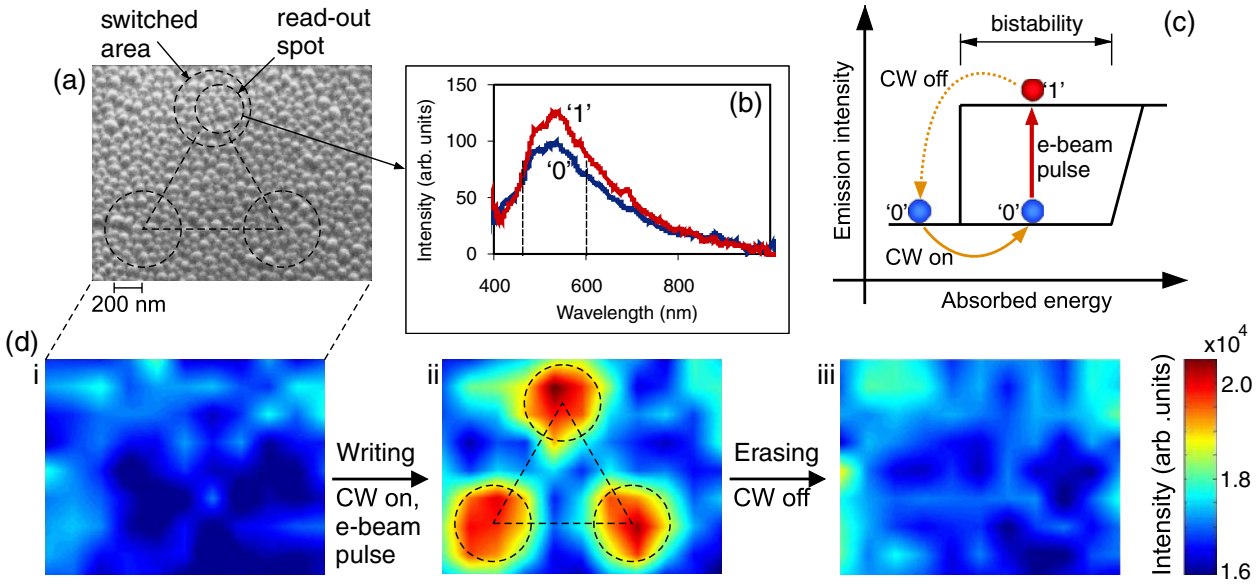

Fig. 8. (Color online) Selective electron-beam-induced switching and CL readout of memory elements within a gallium nanoparticle film. (a) Secondary electron image of the 2000 x 1600 nm^2 area of nanoparticle film (mean diameter 53 nm) used. (b) Typical CL readout spectra for gallium nanoparticles in states "0" and "1", obtained using 2 keV electrons. (c) Schematic illustration of the temperature hysteresis in gallium nanoparticle optical properties and the volatile mode of phase-change memory functionality based on upon it. (d) Readout scans showing integrated CL emission intensity between 450 and 600 nm from the sample area shown in (a) at different stages of the memory cycle: [i] the entire film in state "0" at low temperature; [ii] after electron-beam-induced switching of three 550 nm diameter spots to state "1" at an elevated film temperature within the hysteresis loop maintained by the presence of cw laser light; [iii] after erasing the switched spots, restoring them to the "0" state by switching off the cw laser (allowing the particles to cool).

excitation, and readout was performed via CL measurements using a low-power 2 keV electron beam.

The gallium nanoparticles were initially stabilized in state "0" at a temperature of 120 K, below their solidification temperature. An initial readout scan over a 2000 × 1600 nm^2 area of the film (11 × 9 sampling points) was performed using a 2 keV, 390 pA electron beam with a spot diameter of ~350 nm, encompassing less than 20 particles [see Fig. 8(a)]. At each point, the CL spectrum was recorded and the emission integrated across the range from 450 to 600 nm to produce the emission intensity map shown in Fig. 8(d-i). The cw 1550 nm laser was then switched on to generate a local temperature increase in the nanoparticle film, bringing them to a point (still in state "0") within their transitional hysteresis loop where excitation-induced phase switching is possible [Fig. 8(c)]. Three spots with diameters of ~550 nm (each encompassing less then 50 particles) with mutual separations of 1 μm (i.e., at the corners of an equilateral triangle) were exposed sequentially to single 5 μs 20 keV electron beam pulses with a current of 130 nA (a fluence of ~60 fJ/nm^2). The CL readout scan described above was then repeated and revealed an increase of at least 15% in the 450–600 nm emission from the spots exposed to the higher power electron beam, and no change in the emission from unexposed areas [Fig. 8(d-ii)], thereby demonstrating the selective switching of three individual memory elements from state "0" to state "1". Switching off the cw 1550 nm laser allows the particles to cool and restores the switched memory elements to the "0" state — a fact confirmed by a third CL readout scan [Fig. 8(d-iii)].

It was noted in the introduction above that the thermodynamic lower limit on the energy required for the solid-to-liquid phase transition in a 50 nm gallium particle is of the order of 20 fJ. In contrast, the experiment described here employs a writing electron beam pulse with an energy per particle around three orders of magnitude higher than this. However, one must consider both the relatively small percentage of the electron's energy absorbed by a particle: the energy absorption coefficient for a 20 keV electron beam in a 13.5 nm thick homogenous gallium film (the equivalent mass thickness of the gallium nanoparticle film) is less than 1% (according to formulae from Kanaya and Okayama[34]), and the fact that not all of this energy will go towards heating the particle (some is reradiated in the form of secondary electrons and photons).

6. Enhancement of Logic State Contrast

Several mechanisms, primarily transition radiation and plasmon-mediated emission, contribute to the electron-beam-induced visible and near-IR light emission of nanoparticles.[29] Denisyuk *et al.*[28] touch on this subject and present calculated emission spectra for a single 60 nm spherical gallium particle in vacuum. Such calculations are consistent with the experimentally observed difference of around 15% between solid and liquid state emission reported above. For practical data storage applications, to facilitate error-free readout, it would be beneficial to maximize the contrast between phase (logic) states.

To this end, metallic nanoshells (surrounding a dielectric or semiconductor core) may be considered. These structures are known for the exceptional tunability of their plasmon resonances, which is achieved by varying the core and shell diameters or changing the surrounding medium.[49]

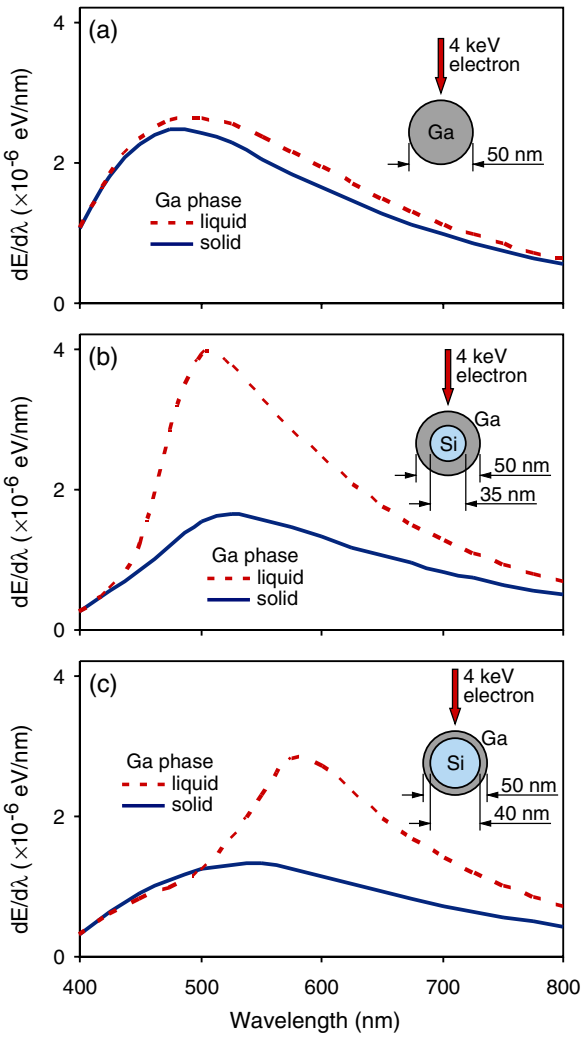

Fig. 9. (Color online) Calculated total CL emission (in all directions) from a free-standing spherical (solid/liquid) pure gallium particle (a), and silicon core–(solid/liquid) gallium shell particles (b, c) in vacuum, induced by a single 4 keV electron with a trajectory through the center of the particle.

The high sensitivity of the nanoshell resonances to these parameters results from the coupling between surface plasmons on the inner and outer metallic surfaces.[50] One may thus hypothesize that the electron-beam-induced emission contrast for phase-change memory read-out might be enhanced through the use of nanoshells in place of homogenous particles.

To test this idea, calculations of electron-beam-induced emission were performed for 50 nm pure gallium nanoparticles and gallium nanoshells of the same outer diameter using the boundary element method.[51] Figure 9 shows emission spectra for 4 keV electrons passing through the centers of free-standing solid and liquid pure gallium nanoparticles and nanoshells of different thicknesses on a silicon core. Dielectric constants for fractionally disordered α-gallium with an optical conductivity similar to β-gallium[30] were used for the solid phase (an approximation to those of β-gallium, which are not available elsewhere). Dielectric constants for liquid gallium were taken from Teshev and Shebzukhov.[33] The calculations show that the difference between solid- and liquid-phase light emission from a 50 nm diameter pure gallium nanoparticle is less then 20%. However, a gallium nanoshell with an outer diameter of 50 nm can exhibit much higher contrast between phases (more than 100% for certain core diameters).

7. Conclusions

The intriguing possibility of high-density nanoparticle phase-change memory has been demonstrated using an electron beam, with intrinsic nanoscale focusability, as a writing tool and a probe. It has been shown that the phase state of bistable gallium nanoparticles can be controlled by electron beam excitation and identified via measurements of their cathodoluminescent emission. With optically distinguishable phase states energetically spaced by as little as 3×10^{-4} eV/atom, femtojoule per particle switching energies are theoretically possible. Indeed, it has already been demonstrated that picojoule single-pulse optical excitations can switch a single particle among a number of different phase (logic) states.

In reviewing this new conceptual basis for memory functionality the electron-beam-induced light emission from bulk gallium in its α (solid) and liquid phases has been studied. Here, for 40 keV electrons, an increase in emission intensity of up to 50% is observed when the metal undergoes a solid-to-liquid phase transition. This result is found to be consistent with calculations of transition radiation for the two phases.

An investigation of the factors affecting the formation of gallium nanoparticles from atomic beam by light-assisted self-assembly has also been performed. In keeping with a model based on a combination of light-enhanced desorption and light-suppressed adsorption, experiments reveal a decrease in mean particle diameter (from 68 to 45 nm) with increasing infrared substrate excitation intensity (from 160 to 630 W/cm^2) during deposition, and the production of larger particles with a narrower size distribution for longer deposition times.

Volatile mode, selectively electron-beam-addressed, rewritable memory functionality, with closely spaced memory elements (comprising less than fifty 53 nm particles each) has been demonstrated in a gallium nanoparticle film. Several individual bits of information were recorded in the structural phase of the gallium nanoparticles using a 20 keV electron beam pulse and read out via measurements of their cathodoluminescent emission in response to a 2 keV electron beam.

Finally, the possibility of enhancing emission contrast for cathodoluminescent readout of phase-change memory by employing nanoshells as opposed to homogenous nanoparticles has been analyzed numerically. Calculations suggest that the electron-beam-induced emission intensity for silicon/gallium core/shell structures may increase by as much as 100% following a solid-to-liquid transition in the gallium shell, as compared to the 15% change observed experimentally for pure gallium particles.

Acknowledgments

The authors would like to acknowledge the support of the Engineering and Physical Sciences Research Council (UK) and EU-FP6 project number NMP4-2006-016881 “SPANS”.

1) R. Kirchain and L. Kimerling: Nat. Photonics **1** (2007) 303.
2) A. Jenkins: Nat. Photonics **2** (2008) 258.
3) R. Zia, J. A. Schuller, A. Chandran, and M. L. Brongersma: Mater. Today **9** (2006) Nos. 7–8, 20.
4) E. Ozbay: Science **311** (2006) 189.
5) D. Pacifici, H. J. Lezec, and H. Atwater: Nat. Photonics **1** (2007) 402.
6) M.-S. Hu, H.-L. Chen, C.-H. Shen, L.-S. Hong, B.-R. Huang, K.-H. Chen, and L.-C. Chen: Nat. Mater. **5** (2006) 102.
7) P. Ahonen, D. J. Schiffrin, J. Paprotny, and K. Kontturi: Phys. Chem. Chem. Phys. **9** (2007) 651.
8) Y. Leroux, E. Eang, C. Fave, G. Trippe, and J. C. Lacroix: Electrochem. Commun. **9** (2007) 1258.
9) M. Wuttig: Nat. Mater. **4** (2005) 265.
10) N. I. Zheludev: Nat. Photonics **1** (2007) 551.
11) A. V. Krasavin and N. I. Zheludev: Appl. Phys. Lett. **84** (2004) 1416.
12) M. Rini, A. Cavalleri, R. W. Schoenlein, R. Lopéz, L. C. Feldman, R. F. Haglund, L. A. Boatner, and T. E. Haynes: Opt. Lett. **30** (2005) 558.
13) K. F. MacDonald, V. A. Fedotov, and N. I. Zheludev: Appl. Phys. Lett. **82** (2003) 1087.
14) M. Bernasconi, G. L. Chiarotti, and E. Tosatti: Phys. Rev. B **52** (1995) 9988.
15) N. R. Comins: Philos. Mag. **25** (1972) 817.
16) A. Di Cicco: Phys. Rev. Lett. **81** (1998) 2942.
17) A. Defrain: J. Chim. Phys. **74** (1977) 851.
18) L. Bosio: J. Chem. Phys. **68** (1978) 1221.
19) R. S. Berry and B. M. Smirnov: J. Chem. Phys. **113** (2000) 728.
20) M. Wautelet: J. Phys.: Condens. Matter **16** (2004) L163.
21) A. S. Shirinyan and M. Wautelet: Nanotechnology **15** (2004) 1720.
22) B. F. Soares, M. V. Bashevoy, F. Jonsson, K. F. MacDonald, and N. I. Zheludev: Opt. Express **14** (2006) 10652.
23) M. Wautelet: J. Phys. D **24** (1991) 343.
24) B. F. Soares, F. Jonsson, and N. I. Zheludev: Phys. Rev. Lett. **98** (2007) 153905.
25) P. D. Townsend, M. Maghrabi, and B. Yang: Nucl. Instrum. Methods Phys. Res., Sect. B **191** (2002) 767.
26) Y. C. Chang, A. L. Cai, A. L. Johnson, J. F. Muth, R. M. Kolbas, Z. J. Reitmeier, S. Einfeldt, and R. F. Davis: Appl. Phys. Lett. **80** (2002) 2675.
27) K. C. Hui, C. W. Lai, and H. C. Ong: Thin Solid Films **483** (2005) 222.
28) A. I. Denisyuk, F. Jonsson, K. F. MacDonald, F. J. García de Abajo, and N. I. Zheludev: Appl. Phys. Lett. **92** (2008) 093112.
29) N. Yamamoto, K. Araya, A. Toda, and H. Sugiyama: Surf. Interface Anal. **31** (2001) 79.
30) O. Hunderi and R. Ryberg: J. Phys. F **4** (1974) 2096.
31) V. L. Ginzburg: Phys. Scr. **T2A** (1982) 182.
32) R. Kofman, P. Cheyssac, and J. Richard: Phys. Rev. B **16** (1977) 5216.
33) R. S. Teshev and A. A. Shebzukhov: Opt. Spectrosc. **65** (1988) 693.
34) K. Kanaya and S. Okayama: J. Phys. D **5** (1972) 43.
35) Y. Lu, G. L. Liu, and L. P. Lee: Nano Lett. **5** (2005) 5.
36) L. Cao, D. N. Barsic, A. R. Guichard, and M. L. Brongersma: Nano Lett. **7** (2007) 3523.
37) T. Ogawa, Y. Takahashi, H. Yang, K. Kimura, M. Sakurai, and M. Takahashi: Nanotechnology **17** (2006) 5539.
38) A. M. Gobin, M. H. Lee, N. J. Halas, W. D. James, R. A. Drezek, and J. L. West: Nano Lett. **7** (2007) 1929.
39) P. C. Wu, T. Kim, A. S. Brown, M. Losurdo, G. Bruno, and H. O. Everitt: Appl. Phys. Lett. **90** (2007) 103119.
40) E. Sondergärd, R. Kofman, P. Cheyssac, and A. Stella: Surf. Sci. **364** (1996) 467.
41) H. Brune: Surf. Sci. Rep. **31** (1998) 125.
42) H. Brune, M. Giovannini, K. Bromann, and K. Kern: Nature **394** (1998) 451.
43) S. Y. Park, T. Isobe, M. Senna, R. A. Weeks, and R. A. Zuhr: Appl. Phys. Lett. **73** (1998) 2687.
44) A. Nahal, H. R. M. Khalesifard, and J. Mostafavi-Amjad: Appl. Phys. B **79** (2004) 513.
45) H. Ouacha, C. Hendrich, F. Hubenthal, and F. Träger: Appl. Phys. B **81** (2005) 663.
46) R. Jin, Y. W. Cao, C. A. Mirkin, K. L. Kelly, G. C. Shatz, and J. G. Zheng: Science **294** (2001) 1901.
47) K. F. MacDonald, V. A. Fedotov, S. Pochon, K. J. Ross, G. C. Stevens, N. I. Zheludev, W. S. Brocklesby, and V. I. Emel'yanov: Appl. Phys. Lett. **80** (2002) 1643.
48) V. A. Fedotov, K. F. MacDonald, V. I. Emel'yanov, and N. I. Zheludev: J. Appl. Phys. **93** (2003) 3540.
49) R. D. Averitt, D. Sarkar, and N. J. Halas: Phys. Rev. Lett. **78** (1997) 4217.
50) E. Prodan and P. Nordlander: Nano Lett. **3** (2003) 543.
51) F. J. García de Abajo and A. Howie: Phys. Rev. B **65** (2002) 115418.